



Aerodynamic and aeroacoustic investigation of an innovative regional turboprop scaled model: numerical simulations and experiments

A. Di Marco¹ · R. Camussi¹ · L. Burghignoli¹ · F. Centracchio¹ · M. Averardo² · M. Di Giulio² · R. Gemma² · E. Pelizzari² · S. Adden³ · P. Aschwanden⁴ · J. Müller⁴ · T. Berkefeld⁵ · S. Haxter⁵ · F. Amoroso⁶

Received: 2 July 2019 / Revised: 18 November 2019 / Accepted: 7 January 2020 / Published online: 23 January 2020
© Deutsches Zentrum für Luft- und Raumfahrt e.V. 2020

Abstract

An extensive aeroacoustic and aerodynamic investigation of an innovative regional turboprop aircraft has been carried out experimentally and numerically under the framework of two research projects funded by the European Union through the CleanSky Research Programme. Experimental tests have been performed in the RUAG Large Subsonic Wind Tunnel in Switzerland and CFD results have been validated against the experimental data. The A/C high-lift performance, stability and control derivatives, aerodynamic noise sources, and low-noise solutions for high-lift devices, have been investigated under representative conditions in cruise, take-off, and landing configurations. The aerodynamic and aeroacoustic investigation has been carried out parametrically, in terms of several reference quantities, including the propellers' thrust and rpm, the speed of the air-flow, the incidence angle of the aircraft and the position of the microphone array used for the acoustic investigation. The present paper gives an overview of relevant results obtained for selected aircraft configurations which have been tested in the wind tunnel and analyzed through CFD simulations. The focus lies on the overall aerodynamic characterization and on the noise sources identification carried out using standard beamforming techniques.

Keywords Wind tunnel · CFD · Propeller · Beamforming

Abbreviations

c_T	Thrust coefficient (–)
D	Propeller diameter (m)
f	Frequency (Hz)
h	Height (m)
J	Advance ratio (–)
n	Rotational speed (1/s)
V_{tip}	Blade tip velocity (m/s)
U	Air velocity (m/s)
α	Angle of attack (°)
θ	Propagation angle (°)

1 Introduction

Throughout the late 1970s and early 1980s, NASA engineers worked on an effort dubbed “the Advanced Turbo-prop Project”, a US government-funded study to examine the feasibility of developing the turboprop engine as a viable competitor to the larger, less efficient turbojet and turbofan designs found on airliners of the day. The studies showed that the turboprop configurations were very efficient at cruise speeds up to about Mach 0.65, providing fuel burn savings between 10 and 20% compared to equivalent turbofan aircrafts. But, above this speed, the increased drag, due to compressibility losses on the propeller blades, caused efficiency to fall rapidly [1]. The use of thinner airfoils and shaping of the blades increases the Mach number at which the drag rise occurs (see e.g. the early works in [2, 3]). But, metal propeller technology did not allow the fabrication of the necessary very thin blades and the development of high-speed turboprop aircrafts stopped in favor of turbofan configurations. Today, with the use of composite materials and advanced design techniques, these limitations can be overcome and economical operations at high subsonic conditions (up to

✉ A. Di Marco
alessandro.dimarco@uniroma3.it

¹ University of Roma TRE, 00146 Rome, Italy

² Leonardo Company, 80038 Naples, Italy

³ IBK Innovation GmBH & Co. KG, 21129 Hamburg, Germany

⁴ RUAG Aviation, 6032 Emmen, Switzerland

⁵ German Aerospace Center DLR, 37073 Göttingen, Germany

⁶ EuroTech Sas, 80125 Naples, Italy

$M=0.8$) seem to become viable (see among many [4, 5]). As a consequence, interest in the turboprop aircraft, with its lower operating cost and fuel efficiency, has increased again. This is widely demonstrated by the strong interest that the main international companies are dedicating to the design of advanced propeller and open fan aircraft [6, 7]. The main research branches are focused on the design of high efficiency and low-noise configurations, on the fuselage noise attenuations for passenger comfort, on innovative design of highly efficient propellers/fans, and on the optimization of the engine-airframe integration. Aircraft noise is also getting major attention by the scientific community in an effort to reduce sky-traffic acoustic pollution, especially in the airport area. Aircraft landing gear, propeller and high-lift devices (HLD) have been recognized as major contributors to the total aircraft noise, especially during landing and take-off. Attention has therefore shifted from the low-noise engines to the study of the airframe generated noise. This is particularly challenging for turboprop aircraft configurations because of the large interaction between the slipstream generated by the propeller blades and the wings/airframe, as well as between the landing gears and fuselage.

This paper deals with the aerodynamic and aero-acoustic characterization of a full-scale regional turboprop by means of experimental tests with a 1:6.5 scaled wind tunnel model and simulations. The numerical and experimental tests have been carried out under two projects funded by the European Union, namely LOSITA and WITTINESS. The target is to advance and develop technologies for both conventional and innovative configurations of future regional turboprop aircraft.

The aerodynamic test campaign in the frame of project LOSITA, carried out on a large-scale powered aircraft (A/C) model in Wind Tunnel (WT) conditions representative of the actual environment in take-off, first climb, and landing phases, did provide a reliable assessment of the low-speed performances of an advanced wing design with respect to the state-of-art. The corresponding acoustic test campaign within the project WITTINESS did allow a deeper characterization of the propeller noise and of the airframe noise, this latter especially related to a novel low-noise design of the flap.

Relying upon the outcomes of these projects, in the frame of the on-going EU-funded CS2 REG-IADP (Clean Sky 2 Regional innovative Aircraft Development Platform) research programme, an adaptive wing concept, and an advanced low-noise propeller design are under maturation process as part of critical technology elements of next-generation regional Turboprop aircraft.

The experimental campaigns have been carried out in a large-scale wind tunnel (WT) that has been previously qualified from the acoustic viewpoint [8]. Tests were performed

on the complete and powered scaled aircraft model in clean, take-off (TO) and landing (LA) configurations the main objective of the investigations being the following:

- validate the A/C high-lift aerodynamic performances in TO and LA configurations;
- characterize the A/C airframe noise in LA configuration and validate low-noise high-lift device (HLD) solutions, including a “lined flap” [9] architecture;
- generate an aerodynamic and acoustic data-base to be used as a reference for validating numerical tools.

Using global measurements of the A/C loads as well as local surface pressure measurements, the aerodynamic characterization has been carried out both experimentally and numerically. The commercial code CFD++ provided the aerodynamic loads for both free flow and wind tunnel conditions.

The objectives of the acoustic study were to determine the magnitude, position, and frequency content of the dominant noise sources and to generate an experimental database for numerical comparisons. According to procedures outlined in the literature (e.g. Refs. [10–12]), the A/C noise sources have been identified and quantified through the application of beamforming techniques to data obtained from a phased microphone array.

Measurements were performed for different angles of attack (AoA), propeller settings (blade pitch, rpm), and positions of the microphone array relative to the model. More details about the experimental set-up and the numerical approach can be found in the next Sect. 2. The main results of both the aerodynamic and aeroacoustic study are given in Sect. 3. The last paragraph, Sect. 4, provides the final remarks and main conclusions.

2 Experimental and numerical methods

2.1 Wind tunnel facility

Experiments were performed in the closed return large subsonic wind tunnel of RUAG in Emmen (LWTE). The hard-walled test section of the wind tunnel has a cross section of 7 m by 5 m and is not acoustically treated. The maximum free stream velocity of the flow is $U_{\max} = 68$ m/s corresponding to $Ma=0.2$. The airflow at atmospheric condition is produced by two counter rotating 8-bladed fans of 8.5 m diameter, which are located in the return path of the tunnel. The LWTE also provides a suitable hydraulic infrastructure to drive the model propellers through hydraulic motors.

The powered aircraft model used in the tests was mounted from the ceiling of the tunnel through a strut. The experimental campaigns included aerodynamic measurements,

using a model internal 6-component balance and pressure taps. For acoustic tests, a microphone array [8] mounted on a movable platform located on the floor of the wind tunnel test section was used.

From the point of view of the acoustic investigation, it must be remarked that closed test section wind tunnels are nowadays regularly used for acoustic array measurements, even though open jet wind tunnels would be preferred since they allow out-of-flow far-field acoustic measurements, improving the individual microphone signal-to-noise ratio [13]. Recent research activities demonstrated that phased array techniques for quantifying airframe noise can be performed in both closed and open jet wind tunnel, providing similar source characteristics (see e.g., [10, 11]). It has been shown that for open-jet wind tunnels additional flow-induced disturbances may affect the reliability of acoustic measurements carried out with phased microphones array. The possibility to perform acoustic measurements in parallel to aerodynamic tests in the same wind tunnel presents financially interesting synergies.

2.2 The instrumented and powered scaled model

Tests have been performed on a complete A/C model powered by two wing-mounted engine simulators. Based on the thrust/power requirements and previous experience by the wind tunnel operator, a propulsion solution using hydraulic motors was selected.

The main length-scales of the A/C model are: 4.7 m span, 4.8 m length, 1.5 m height. The model is representative of a 1:6.5 scaled regional aircraft turboprop developed by Leonardo Company and Alenia.

The design of the wind tunnel model was driven by the goal to achieve high testing efficiency and flexibility. Figure 1 documents the general architecture of the model with the main modules highlighted. The wings consist of part-span single slotted flaps, spoilers, ailerons, and winglets. For the tests, the inboard and outboard flap components were set at deflections representatives of the clean, TO and LA configuration. The T-tail empennage consisted of two elevators on the horizontal plane and a rudder on the vertical one. The angle of attack and the sideslip angle were set and controlled by the pitch drive of the model support system.

Figure 2 shows the model installed in the LWTE test section with the dorsal strut used for the aero-acoustic campaign and the ventral strut for the aerodynamic identification part.

The model is equipped with two eight blades propellers. The blade pitch angles are manually adjusted and the propellers are powered by RUAG MG20 hydraulic engines (75 kW, 10,000 rpm). The hydraulic power station drives these motors individually and keeps the propellers at a fixed rpm.

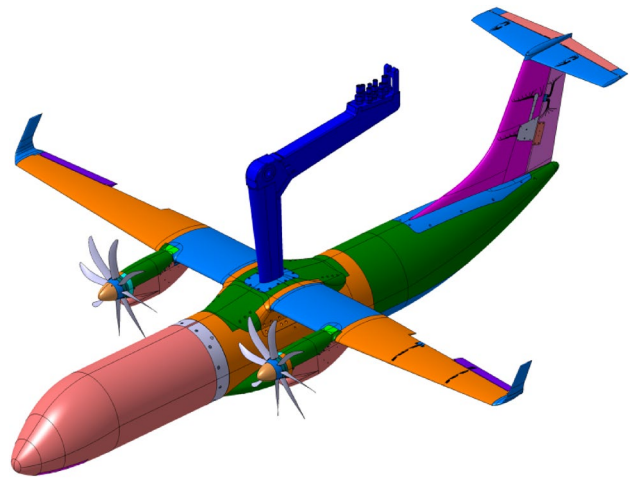


Fig. 1 CAD drawing of the complete model with the different modules highlighted (the main modules are: fuselage, tail, nacelle/engine and wings)

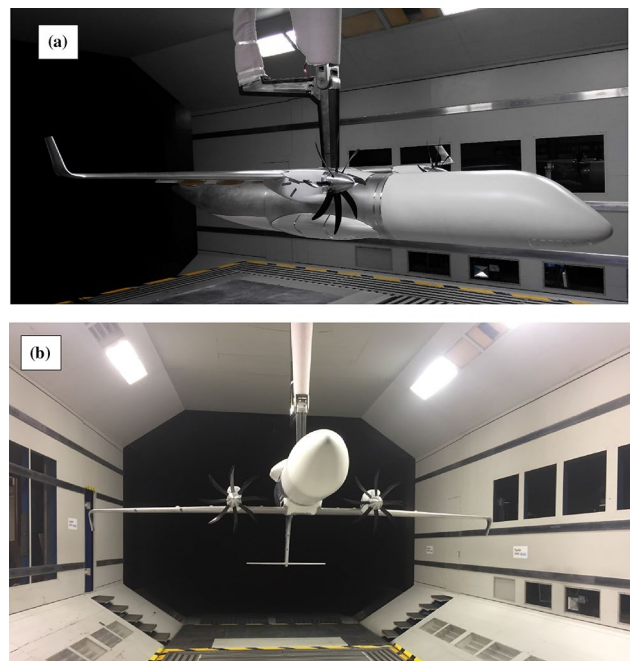


Fig. 2 The powered WT-Model installation: **a** dorsal installation for the acoustic measurements; **b** ventral installation for the aerodynamic measurements

2.3 Measurement equipment and procedure

The acoustic measurements were carried out using a planar microphone array (visible at the bottom of Fig. 2a) composed of 144 electret microphones arranged in a 40mm thick aluminum plate. All microphones are recessed behind a conical opening in order to reduce the influence of wall pressure fluctuations caused by the turbulent boundary-layer

and in general to improve the signal to noise ratio. The array has a maximum aperture of 1.5m and is placed on the test section floor. The 144 array microphones were connected to four GBM VIPER HDR multi-channel data acquisition units equipped with 24bits A/D conversion boards. Data are acquired at a sampling frequency of 150 kHz for a period of 30 s per test point. All channels were equipped with anti-aliasing filters with a cut-off frequency of 70kHz. To reduce the low frequency noise of the WT, a second-order high-pass filter [14] with adjustable cut-off frequency was set to 500Hz. Microphone signals were processed by applying the cross-spectral estimation by Welch using a window length of 2048 samples, an overlap of 50%, and a Hanning weighting window.

Maps of local sound pressure contributions were obtained by applying a frequency domain beamforming technique that includes the diagonal removal technique [13] and the subtraction of a background noise matrix obtained from an empty WT measurement (strut installed). The source maps were calculated in 1/3rd octave bands by integrating the narrowband maps between the upper and lower frequency limits of each band. Among the variety of beamforming algorithms developed in the past (the reader may refer to Refs [15–16], for an overview) the CLEAN-SC [18] deconvolution procedure was selected to enhance the sound maps.

To quantify the noise level of the propellers, a source power integration procedure (SPI) was used to compute the narrow-band and third-octave acoustic spectra

generated from a selected region on the model. The simplified method without auto-powers, presented in Ref. [19], is used. In order to avoid unphysical contributions, grid point results with negative amplitude or a level below more than 12dB of the peak [10] are excluded from the integral calculation. Absolute source contributions using CLEAN-SC are calculated as well on the same scan area and compared to the SPI integration results. Two scan planes were chosen for analysis. One was located roughly in the plane of the wing and the other was located in the plane of the landing gear. A sketch of the two planes is shown in Fig. 3. In the following description, the origin of the frame of reference is assumed at the center of the WT test section. The positive x -axis is aligned to the direction of the air flow, the y -axis is in the cross-wise direction and the z -axis is perpendicular to the WT test section floor (pointing up, the right hand rule applied).

A 40 points scan-grid that covers the full model was used for a preliminary evaluation and determination of the local sound levels. It covers an area $6.5 \text{ m} \times 5.2 \text{ m}$ wide with a grid spacing of $\Delta x = \Delta y = 0.03 \text{ m}$ centered at the origin of the test section frame of reference. On the basis of this preliminary noise source analysis, smaller subset areas were successively selected for the purpose of analyzing the noise sources in more details. In these cases, the region of interest is scanned with a spatial resolution of $\Delta x = \Delta y = 0.01 \text{ m}$. The full model and the subset areas are shown in Fig. 4. For all test points, the scan grid is rotated with the AoA of the model.

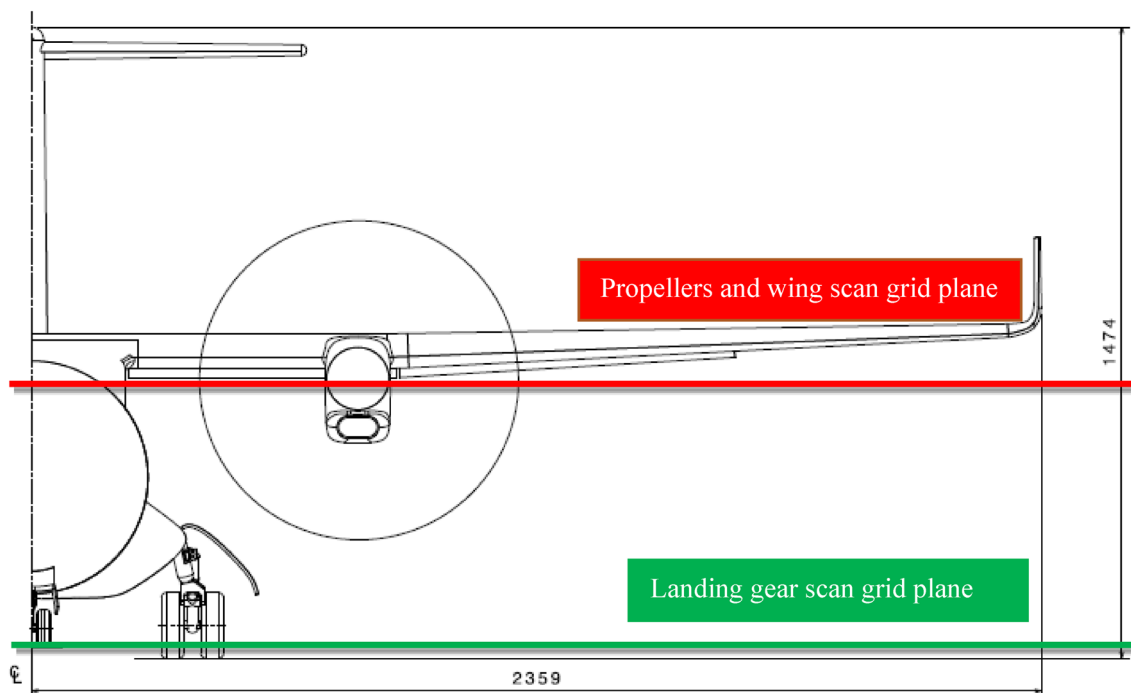
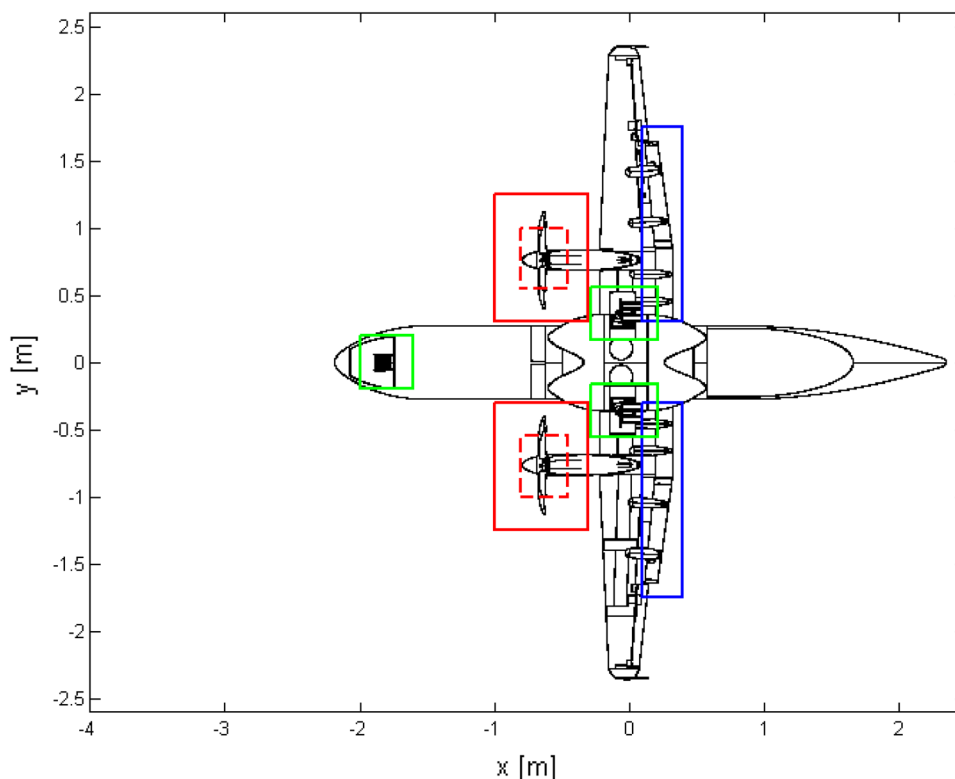


Fig. 3 Front view of the wind tunnel model with the two horizontal planes used for the scan grids

Fig. 4 Scan grid areas and noise source regions of interest: in red the propeller regions, in green the landing gear regions and in blue the flaps regions



For the aerodynamic test campaign, global forces and moments are measured through the RUAG six-component balance. The static pressure distributions are obtained from several rows of pressure taps installed on the left (instrumented) wing, horizontal tail, vertical tail, and fuselage. Forces acting on the propellers are measured as well using a rotating shaft balance. The wind tunnel results are corrected to take into account blockage effects and to reproduce the free air case. Experimental results will be compared and discussed with corresponding CFD calculations in the next sub-section.

2.4 Aerodynamic and aeroacoustic measurements test matrix

To allow extrapolation of the results to full scale, the experiments were ideally performed at the same advance ratio and the same tip Mach number as the real conditions, thus the propeller thrust was not fixed to compensate the model drag.

The acoustic measurements were conducted without the landing gears and the tail assembly (empennage) in order to better characterize the noise behavior of the propellers and of the airframe. The strut from the ceiling and the pitch actuator were covered with fabric to better absorb impinging acoustic waves. The acoustic measurements for the propeller characterization were made with the model at a fixed angle of attack ($\alpha = 6^\circ$) and flow speed ($U_{inf} = 50$ m/s), for two rotational speeds and four axial microphone array

positions, corresponding to propagation angles $\theta = -50^\circ, -30^\circ, 0^\circ, +30^\circ$ along the streamwise direction. For each rotational speed, the propeller thrust was adjusted by setting the blades pitch angles accordingly (details of the propeller settings are given in Table 1).

To characterize the acoustic behavior of the hydraulic motors, 8 additional test points were added to the propeller noise test campaign. For each array position, at 50 m/s and AoA of 6° , two runs were carried out with the hydraulic motors on and two rotational speeds of the clean hubs without propeller blades. The test matrix used for the engine-on aeroacoustic part of the test campaign is given in Table 1. A separate measurement campaign was devoted to the characterization of the airframe noise without propulsion and to evaluate the effect of the lined flap. The flow conditions analyzed are given in Table 2.

Table 1 Test matrix adopted for the aeroacoustic investigation

Parameter	Values		
A/C model powered			
Propagation angle θ ($^\circ$)	-50, -30, 0, +30		
WT speed U_{nom} (m/s)	50	60	
AoA α ($^\circ$)	+6		
Rotational speed n (rpm)	3550	4205	6020
Blade pitch angle ($^\circ$)	31, 33, 34	27, 28.3, 29	28.3

Table 2 Measurement parameters of the baseline and lined flap LA configuration

Parameter	Values
Lined flaps, LA	
Propagation angle θ ($^\circ$)	$-50, -30, 0, +30$
WT speed U_{nom} (m/s)	30, 50, 68
AoA α ($^\circ$)	0, +6, +8

Table 3 Flight control surface deflections

Control surface	Deflection	
	Maximum	Interval
Aileron	$\pm 30^\circ$	$\pm 15^\circ$
Rudder	$\pm 30^\circ$	$\pm 15^\circ$
Elevator	$\pm 25^\circ$	$\pm 12.5^\circ$
Spoiler	$+60^\circ$	$+30^\circ$

It should be pointed out that, for the sake of conciseness, the effect of the propagation angle θ , and the noise source directivity (both for the propeller and the airframe noise) is not treated in the present paper the reader can refer to Ahlfeldt et al. [20] for more details. The acoustic results presented in the next section are thus limited to the case $\theta = 0^\circ$.

The aerodynamic data base generation measurements are performed at 60 m/s, corresponding to a WT Mach number of 0.176 and a Reynolds number of 1.62×10^6 . For these flow conditions, no laminar boundary layer is expected over the whole model, in agreement with the expected full-scale behavior.

Aerodynamic polars were obtained by varying the incidence angle α from -6° to 20° with 0.25° resolution. Similarly, the sideslip angle β was varied from -15° to 15° with a 0.5° resolution. In addition, deflections of the control surfaces (Aileron, Rudder, Elevator, Spoiler) were varied. The corresponding angular deflections are reported in Table 3.

The main overall configurations tested were the following:

- Clean, no high lift surfaces deployed.
- LA with a 33° flap deployed.
- TO with a 18° flap deployed.

The same configurations and settings were analyzed numerically using the approach that shall be described in the next subsection.

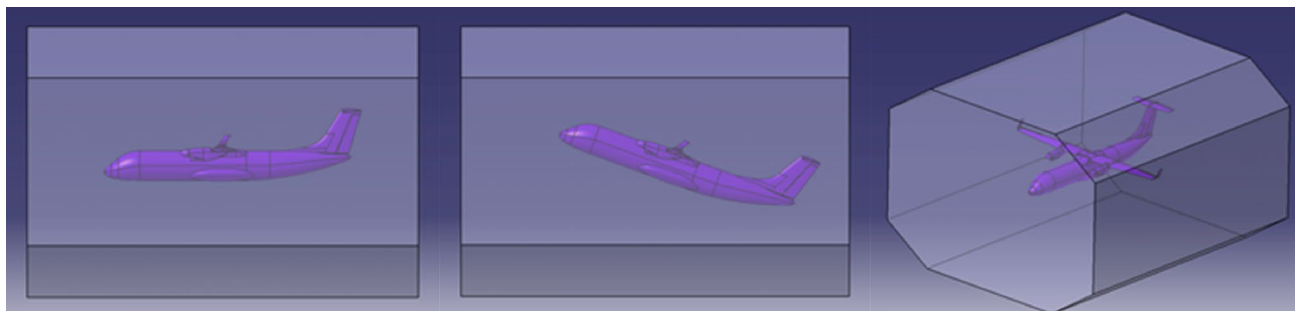
2.5 CFD models and Computational methods

Several numerical simulations were carried out and the results compared against the experimental data thus providing a validation of the adopted numerical approach. Furthermore, the numerical simulations were useful to verify and evaluate quantitatively the blockage effects affecting the WT measurements. To this purpose, two different boundary conditions have been adopted:

- CFD of the scaled model including the Wind Tunnel test section walls (WTS).
- CFD of the scaled model in free air (FA).

Uncorrected wind tunnel results have been compared to the CFD cases with WTS, whereas the corrected wind tunnel results have been compared to the numerical FA cases. The two approaches have been applied for each reference A/C configuration, i.e. the clean, LA and TO.

An example of the computational domain is shown in Fig. 5. The computational model of the A/C has been endowed with control surfaces: movable ailerons, rudder, elevators, and spoilers' surfaces were defined in the CAD model. High lift device fairings have been placed all the configuration. The effect of the propellers has not been modelled. Therefore, comparisons against experiments have been made for power off wind tunnel runs only, i.e., for the model set-up without the propeller blades. This issue also regards the aerodynamic coefficients reported in the following, that do not include the propeller load, both for the experimental and the numerical results.

**Fig. 5** A/C model and computational domain used in the CFD simulations

Computations have been performed at the wind tunnel Reynolds number using the CFD++ solver. Steady 3D RANS simulations were carried out selecting the appropriate mesh after a standard grid refinement procedure. Three-dimensional viscous type unstructured meshes were generated for the numerical solution of the Navier Stokes equations. The mesh is made of about 70 million elements made up of prisms layers near walls (boundary layer) and tetrahedra in outer computational domain. All RANS computations were performed using the SST turbulence model, with an Advanced Two Layer bland mode in equilibrium state wall function, at wind tunnel Mach and Reynolds numbers.

3 Results

3.1 Aerodynamic characterization and CFD comparisons

Simulations were done for clean, take-off and landing and the results compared well with the wind tunnel results. Examples of pressure coefficient (C_p) distributions provided by the CFD analyses are shown in Fig. 6 for the clean (cases a and b), the landing (c and d) and the take-off configurations (e and f) on the upper and lower side of the A/C. The reported C_p demonstrates that the CFD investigation is capable of reproducing the expected behavior over the whole aircraft. The pressure load on the upper side of the wings is indeed higher in the landing and take-off configurations with respect to the clean case and the trace of the propellers nacelle wake is correctly reproduced. Also, the action of the high-lift devices is evident in particular for the landing cases where the induced increase of C_p over the HLD can be clearly observed.

The main results in terms of aerodynamic coefficients for the clean configuration are given as polar in Fig. 7. A comparison between the results of the WT and of CFD analyses performed at the same conditions (Re and Ma) is presented and the agreement between experiments and CFD results is very good. The numerical results correctly predict the maximum lift coefficient as well as the stall AoA. The drag coefficient is also predicted correctly thus supporting the idea that the numerical simulations carefully reproduces the wind tunnel model, that includes the fairings and the movable surfaces.

The polars obtained for the TO configuration are given in Fig. 8. The CFD correctly predicts the stall both in terms of maximum lift coefficient and AoA. Also, the drag coefficients computed in FA correctly approximate the corrected experimental data.

Simulations and measurements at LA are reported in Fig. 9. It is shown that the CFD provides a good estimation

of the maximum lift coefficient and of the $C_{L\alpha}$ slope. On the other hand, the C_D coefficient is well approximated up to the stall incidence, after that an overestimation is present. The comparisons of the WTS/FA computations against the not corrected/corrected experimental data suggest that the adopted wind tunnel corrections are adequate.

Examples of results obtained on the Control Surfaces are reported in Fig. 10. The agreement between experiments and the CFD results is still satisfactory even though some discrepancies are observed in the case of the elevator (case a). A possible explanation can be the effect of the wake of the wing and the fuselage that impacts the tail. This complex behavior cannot be accurately predicted by the RANS simulations and thus leads to some uncertainties in the prediction of the load on this surface. Further analysis is currently underway by the authors to better clarify this point.

3.2 Acoustic investigation

As pointed out above, the noise source identification and characterization has been carried out by the application of the beamforming technique and, for the sake of brevity, the maps reported therein are limited to a few selected conditions representative of situations of interest.

Examples of full grid dirty maps obtained in the engine configuration are given in Fig. 11. The results are presented for the following parameters $U_{nom} = 50$ m/s, $\alpha = 6^\circ$, $\theta = 0^\circ$, $n = 3550$ and $\beta = 34^\circ$, these settings corresponds to a maximum thrust coefficient condition. CLEAN maps on the refined grid located on the left propeller can be found in Fig. 12. The dirty and CLEAN maps are shown for a dynamic range of 15 and 30 dB respectively and four third octave bands. The selected central frequencies span from 5 to 40 kHz and the amplitude of the maxima SPL are reported in the subplot titles. It should be noted that aeroacoustic tests in hard walled closed-section wind tunnels always suffer from multipath sound reflections and that causes the absolute values of the sound pressure levels to be affected by systematic errors that are quite difficult to be estimated and removed. The effect of the potential reflections was estimated in a dedicated preliminary test campaign [8]. It was demonstrated that reflection effects are very unlikely for the model configuration considered and do not affect the results also in view of the acquisition and post-processing parameters chosen. This conclusion was driven by the estimation of the time of reflection assuming a source in the center of the wind tunnel. In account of the size of the test section and the speed of sound it has been demonstrated that reflections are not affecting the processed data.

The full grid dirty maps highlight the dominant sound sources that, in the dynamic range considered, are represented by the propellers. The dirty maps demonstrate that the adopted beamforming technique works well but a more

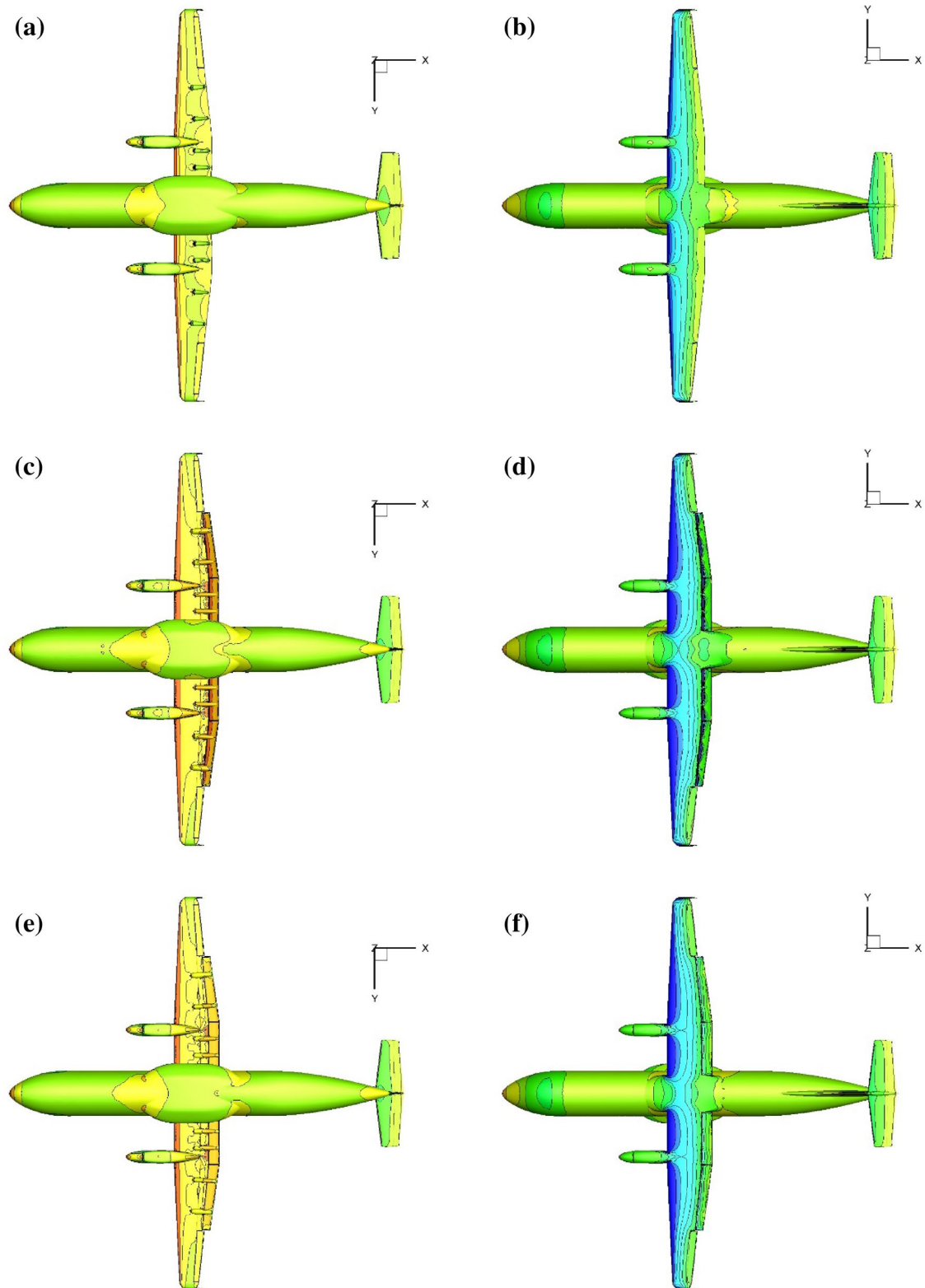


Fig. 6 C_p distribution computed on the A/C at $\alpha = 10^\circ$; upper side (plots on the left) and lower side (plots on the right). **a, b** Clean configuration, **c, d** landing configuration; **e, f** take-off configuration

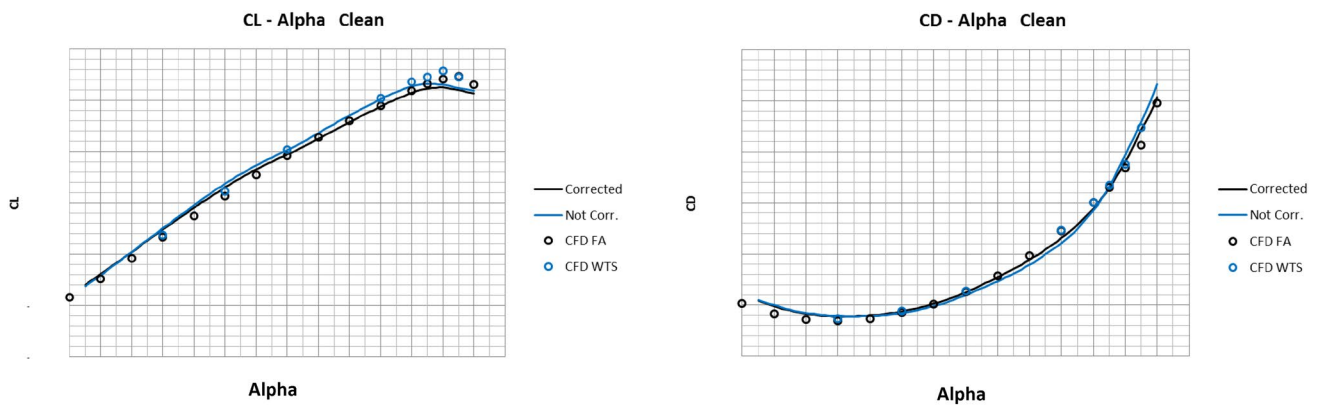


Fig. 7 Lift and drag coefficients comparisons in the clean configuration

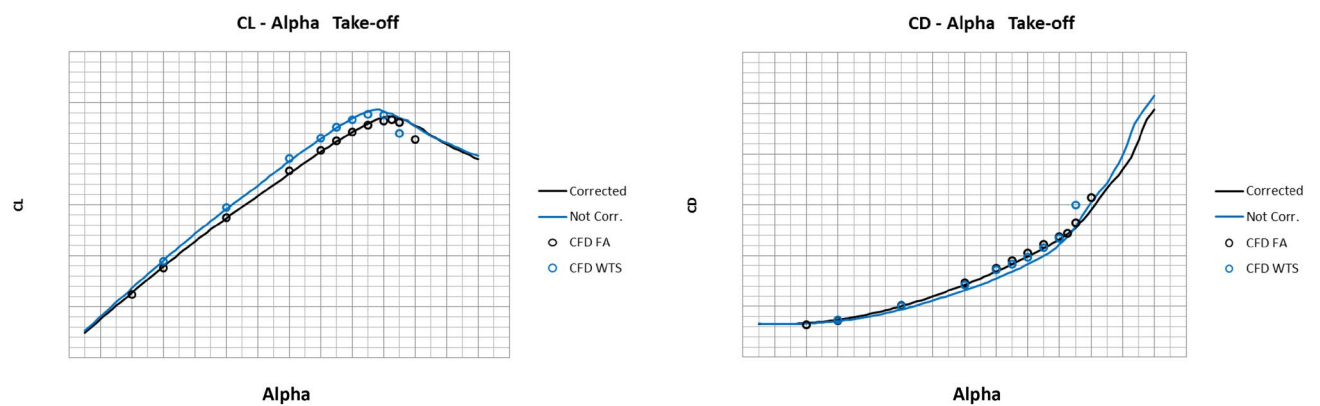


Fig. 8 Lift and drag coefficients comparisons in the TO configuration

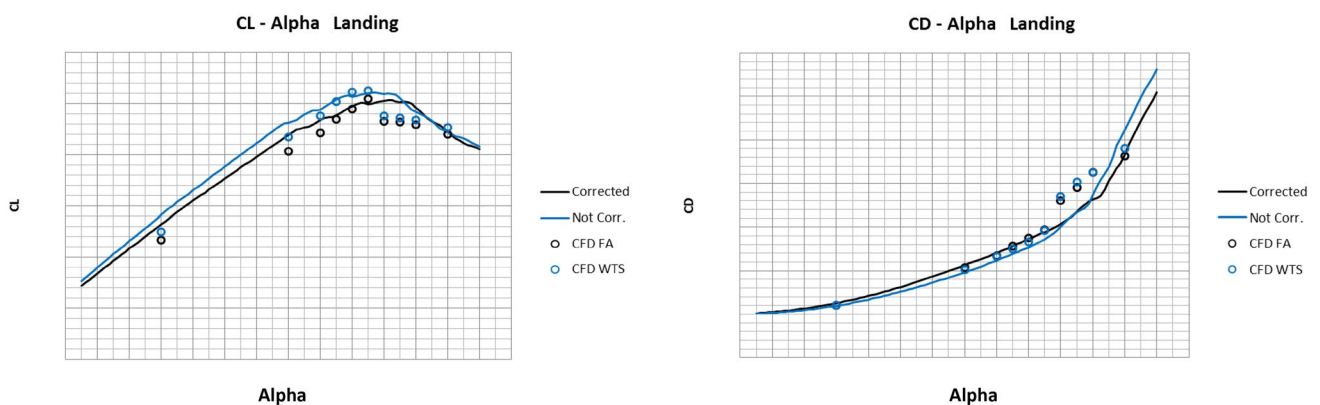


Fig. 9 Lift and drag coefficients comparisons in the LA configuration

precise estimation of the strength and location of the noise sources is obtained by the application of the CLEAN-SC procedure. As expected, the CLEAN maps of Fig. 12 show that the main noise sources associated with the propeller are spread over the rotating blade tip region, multiple

spots representing the passages of the propeller blades. This is an artifact of the adopted beamforming procedure that does not compensate the rotation of the noise source located at the blade tip. Indeed, the noise sources are identified on the propeller side whose blade tips are travelling

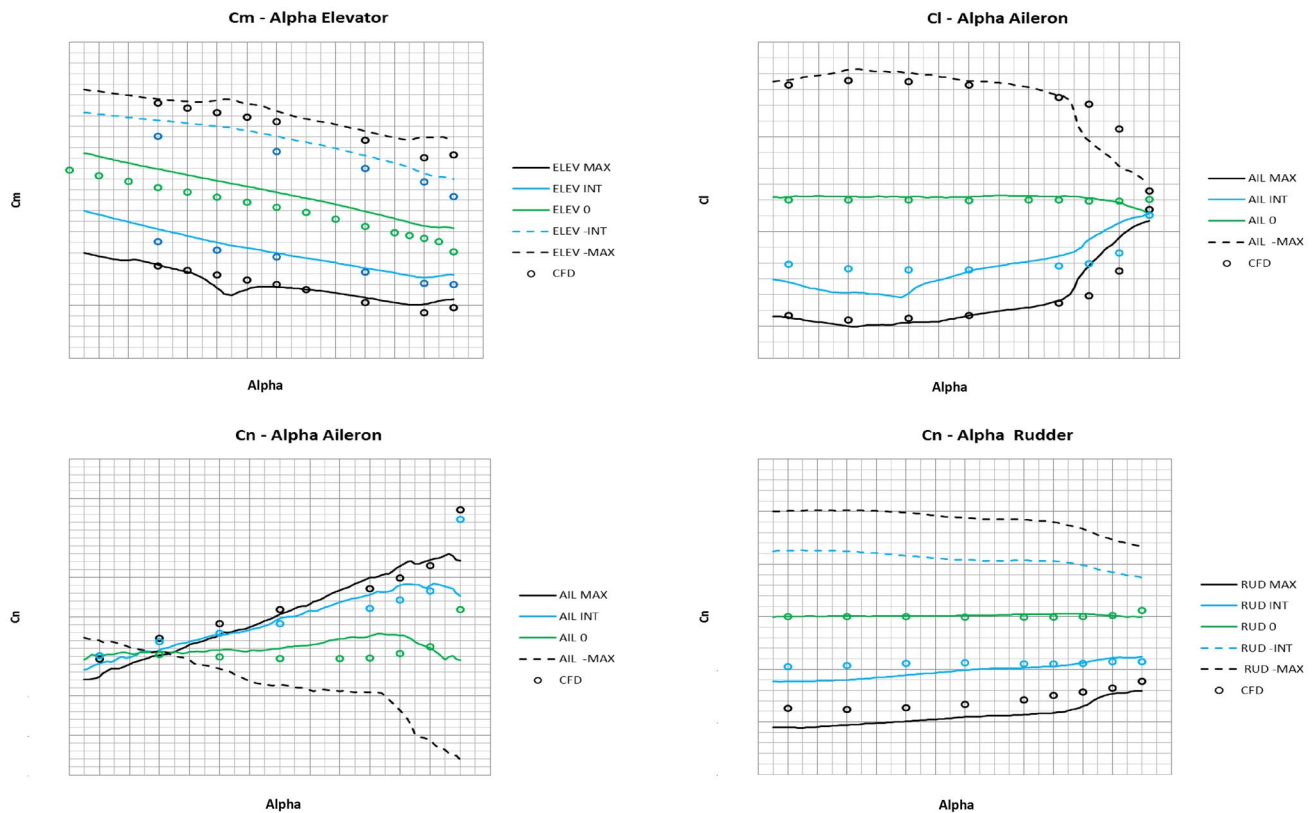


Fig. 10 Explanatory force and moment coefficients computed and measured on representative control surfaces of the scale model

towards the microphone array. Taking into account that the propellers are rotating in counter clock-wise direction, this corresponds to the upper part of the region of interest close to the propeller blades.

Similar results are obtained in the other cases of Table 1, namely at $U_{nom} = 60$ m/s, and an overall representation of the effect of the other relevant parameters, pitch angle and rpm, is provided in Figs. 13 and 14 where the narrow band integrated spectra are reported as SPL as a function of frequency. The spectra are presented in the range between 300 Hz to 40 kHz that comprises the first BPF. Figure 13 reports the effect of the thrust coefficient variation achieved by varying the pitch angle at fixed rotation velocity. It can be observed that for increasing blade pitch angles, the spectral amplitude at the BPF increases whereas the broadband component, being related to the WT boundary layer, remains approximately the same. It should be noted that an increase of the blade pitch angle leads to an increase of the thrust coefficient and of the energy of the flow structures detached from the blades. This behavior induces an increase of the sound levels at the BPF. When the thrust coefficient is fixed at $C_T = 0.135$ (Fig. 14) the BPF is shifted according to the different rpm but the largest energy is achieved again for the highest pitch angle. As for the previous case, the broadband

component of the spectra is weakly affected by the variation of the propeller operating condition.

The dirty and CLEAN maps obtained in a reference configuration ($U_{nom} = 68$ m/s, $\alpha = 0^\circ$) for the airframe noise estimation (power off condition) are shown in Figs. 15 and 16 respectively. As for the previous cases, the dynamic ranges are 15 and 25 dB respectively and four third octave bands. The central frequencies and the maxima SPLs are shown in the figure title.

The full grid dirty maps (Fig. 15) show that the dominant noise sources are located at the fuselage ogive and at the landing gears. Noise sources located on the wings are only relevant at low frequencies, because their signatures disappear for central frequencies higher than 20 kHz. This behavior has been verified through an extensive analysis of the full grid CLEAN-SC, results that are not reported here. Similar results are obtained at lower mean velocities (30 m/s and 50 m/s) and are not reported for brevity.

To better highlight the HLD acoustic effects, a region of interest has been selected around the left wing and the CLEAN-SC technique has been applied. Results are shown in Fig. 16 where the location and strength of the noise sources can be clearly seen. They are mainly localized at the flap and ailerons side edge, the latter becoming dominant at very high frequencies. Other possible sources of noise, such

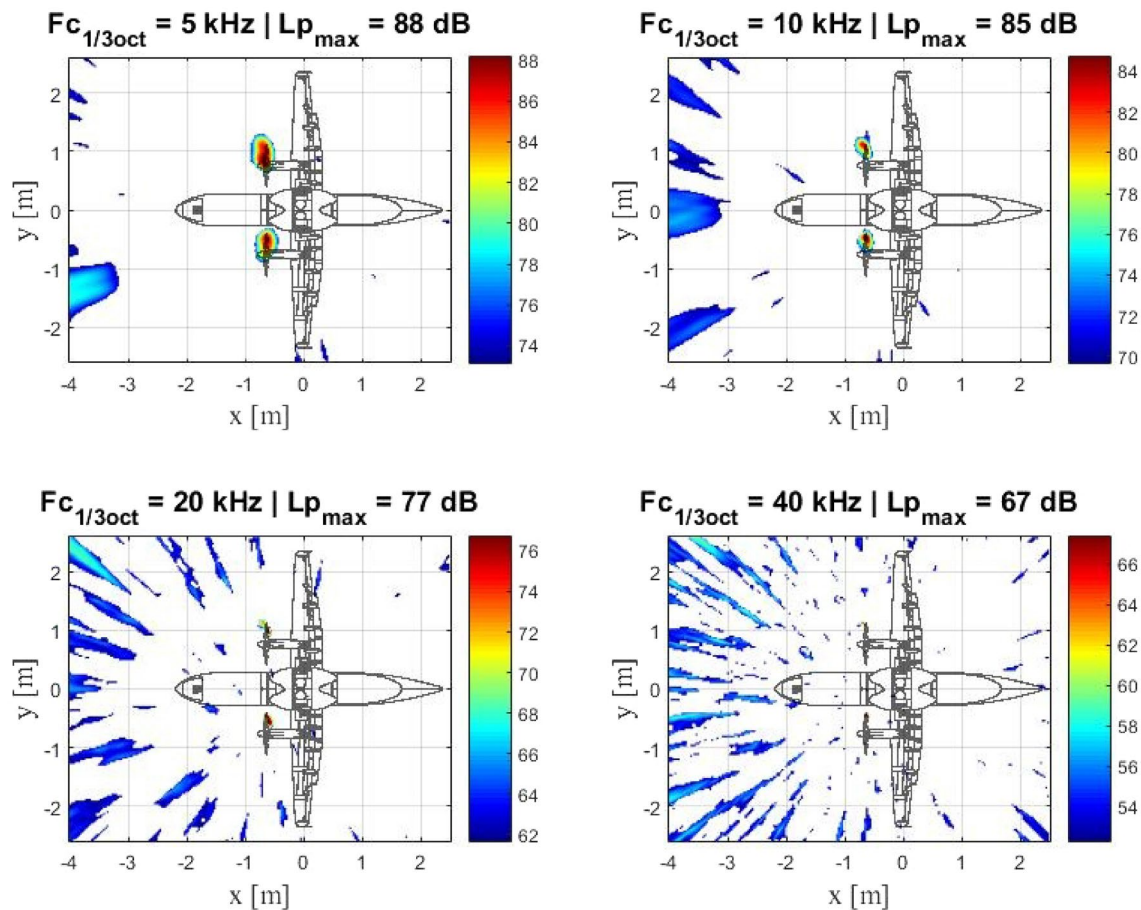


Fig. 11 Third octave dirty maps of the propelled A/C model with the array in overhead position ($\theta=0^\circ$). $U_{\text{nom}}=50$ m/s, $\alpha=6^\circ$, $\theta=0^\circ$, $n=3550$ and $\beta=34^\circ$

as those located at the trailing edge of the wing and of the flaps are indeed present but in the frequency range selected and for the position of the selected scan grid appears to be not relevant.

Similar tests and data processing procedures have been carried out in the configurations equipped with the lined flap. Figure 17 shows a picture of one of the investigated configurations.

In order to quantitatively evaluate the effectiveness of this low-noise device, a direct comparison of the noise source strengths with and without the lined flap installed has been performed. Figures 18 and 19 show the variation of the noise source strengths induced by the lined flap installation as a function of the frequency at three AoAs and for free stream speeds set to 68 m/s and 50 m/s respectively. The variation (denoted as L_p) is estimated by subtracting the spectrum of the low-noise device to the spectrum of the conventional one, at the same conditions. Therefore, a negative value corresponds to a benefit because indicative of a noise reduction. The results are shown over the frequency range of interest. Considering the overall results presented

above, higher frequencies are not relevant in terms of HLD acoustic effects. The acoustic benefits of the lined flaps are clearly evident, in terms of source strength reduction, over the whole frequency range considered. An overall estimation of the benefit has been achieved by averaging L_p over the selected frequency range. The mean difference ranges between -5 dB to -7 dB, the noise reduction being more significant at high AoA and at the lower speed. Similar results have been obtained at 30 m/s but, being less important in terms of the full-scale extrapolation, are not reported therein.

4 Conclusion

The present paper reports results obtained in an extensive experimental and numerical investigation with the goal to aerodynamically and acoustically characterize a powered regional turboprop aircraft. Experiments have been carried out on a 1:6.50 scaled full aircraft model in the RUAG large-scale wind tunnel facility in Emmen. The

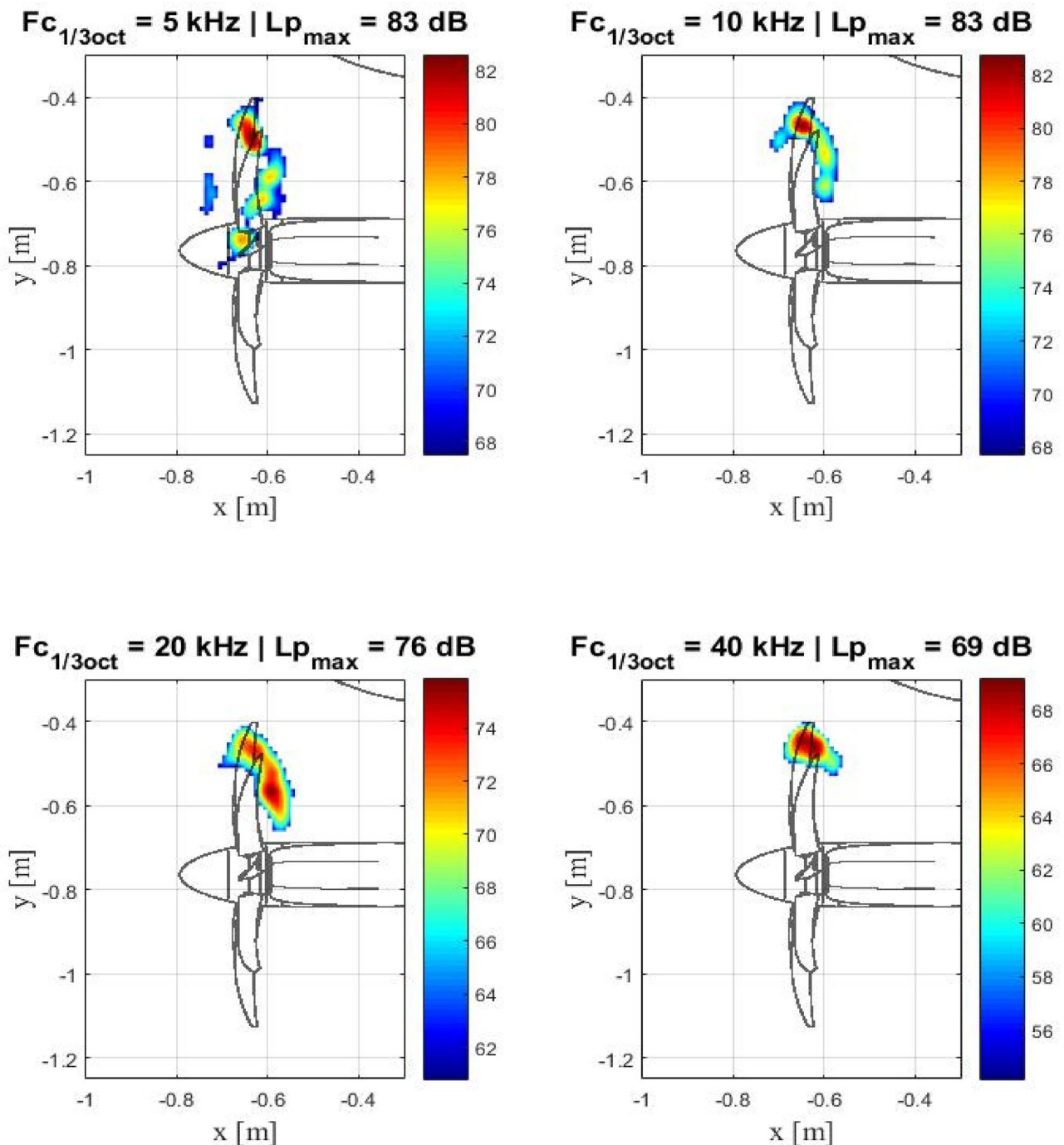


Fig. 12 Third octave CLEAN maps of the left propeller. Conditions are the same as Fig. 11

experimental tests included both aerodynamic and acoustic measurements, the latter using a large microphone array installed on the floor of the wind tunnel test section at different streamwise positions. Numerical simulations have been performed to provide the aerodynamic overall properties of the full A/C and to verify the effectiveness of the control surfaces.

The good agreement of the WTS/FA results with the uncorrected/corrected experimental data shows that even for this large model compared to the test section dimensions, the applied wind tunnel corrections are adequate.

The symmetry of the results indicates that the model and its installation in the wind tunnel are devoid of asymmetries. The analyzed experimental data give an overall description

Fig. 13 SPL integrated spectra for different configurations. Left graph: 3550 rpm; blue line = 31°, black line = 33° and red line = 34° blade pitch angles. right graph: 4205 rpm; blue line = 27°, Black line = 28.3° and red line = 29° blade pitch angles

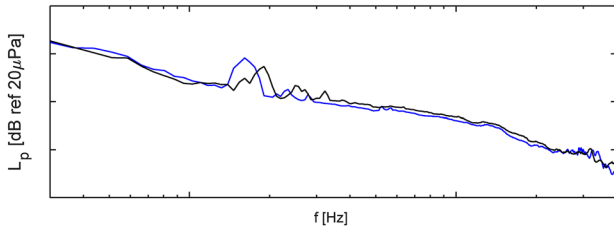
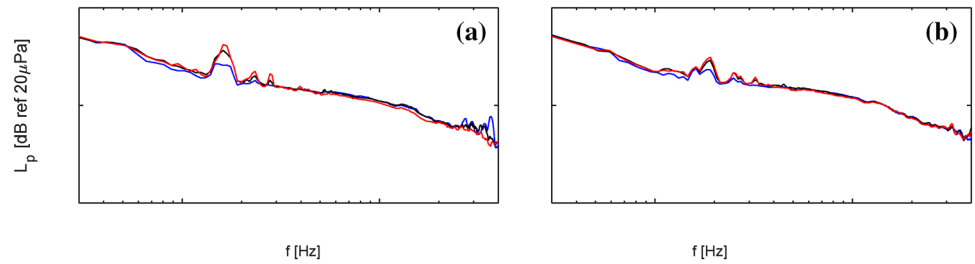


Fig. 14 SPL integrated spectra obtained at the same thrust coefficient ($C_T=0.135$). Blue line: 3550 rpm and 33° blade pitch angle. Black line 4205 rpm and 29° blade pitch angle

of A/C characteristics and neither aerodynamic design flaws nor measurements errors are noticeable for the considered test configurations.

A good match between experimental values and CFD has been found for the three examined configurations and satisfactory results emerged in the analysis of the control surfaces aerodynamic properties where, in some cases, the CFD does not correctly predict the aerodynamic coefficients.

The aeroacoustic behavior was studied by applying beamforming techniques to fluctuating pressure signals

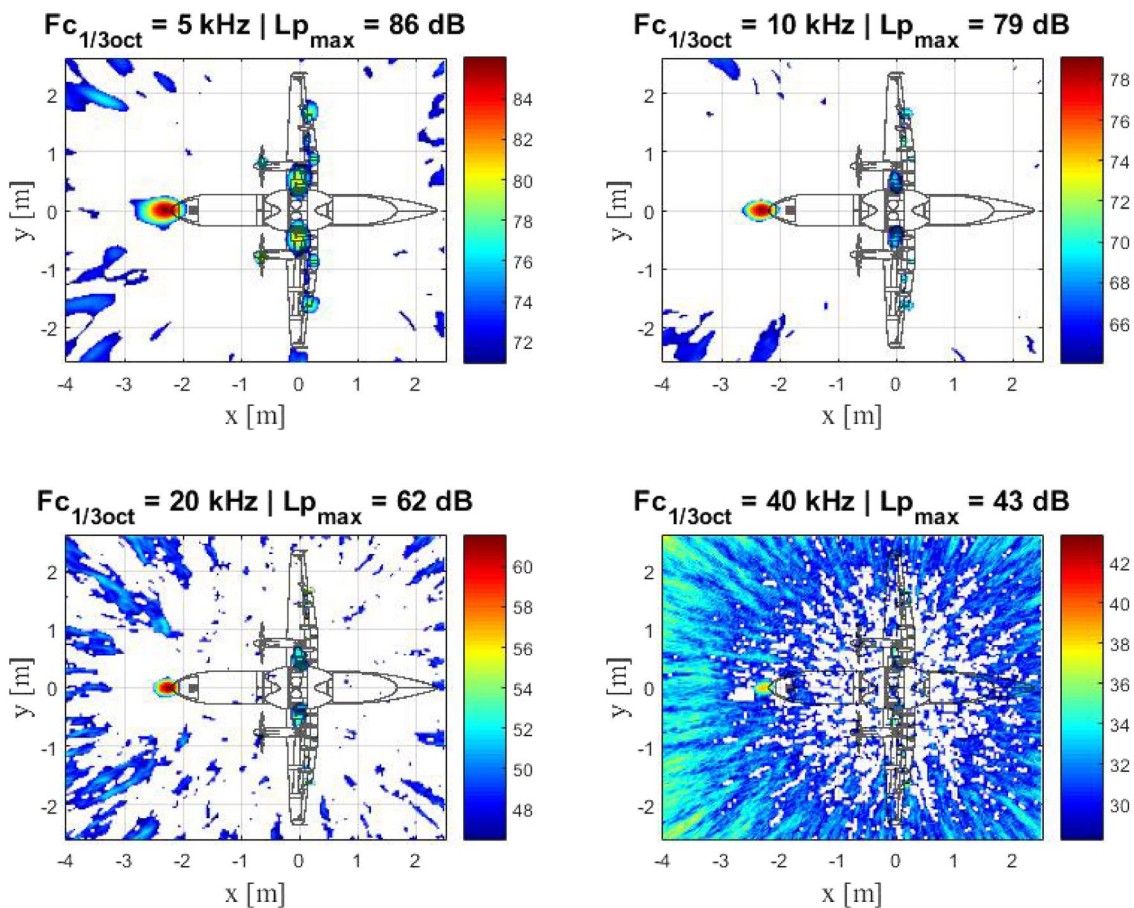


Fig. 15 Full Grid Source maps for the test case with $U_{nom}=68$ m/s, $\alpha=0^\circ$, $\theta=0^\circ$, baseline LA configuration, flaps plane $z=0.18$ m

Fig. 16 Clean maps for the same condition of the previous figure but for a region of interest refined on the left wing flaps

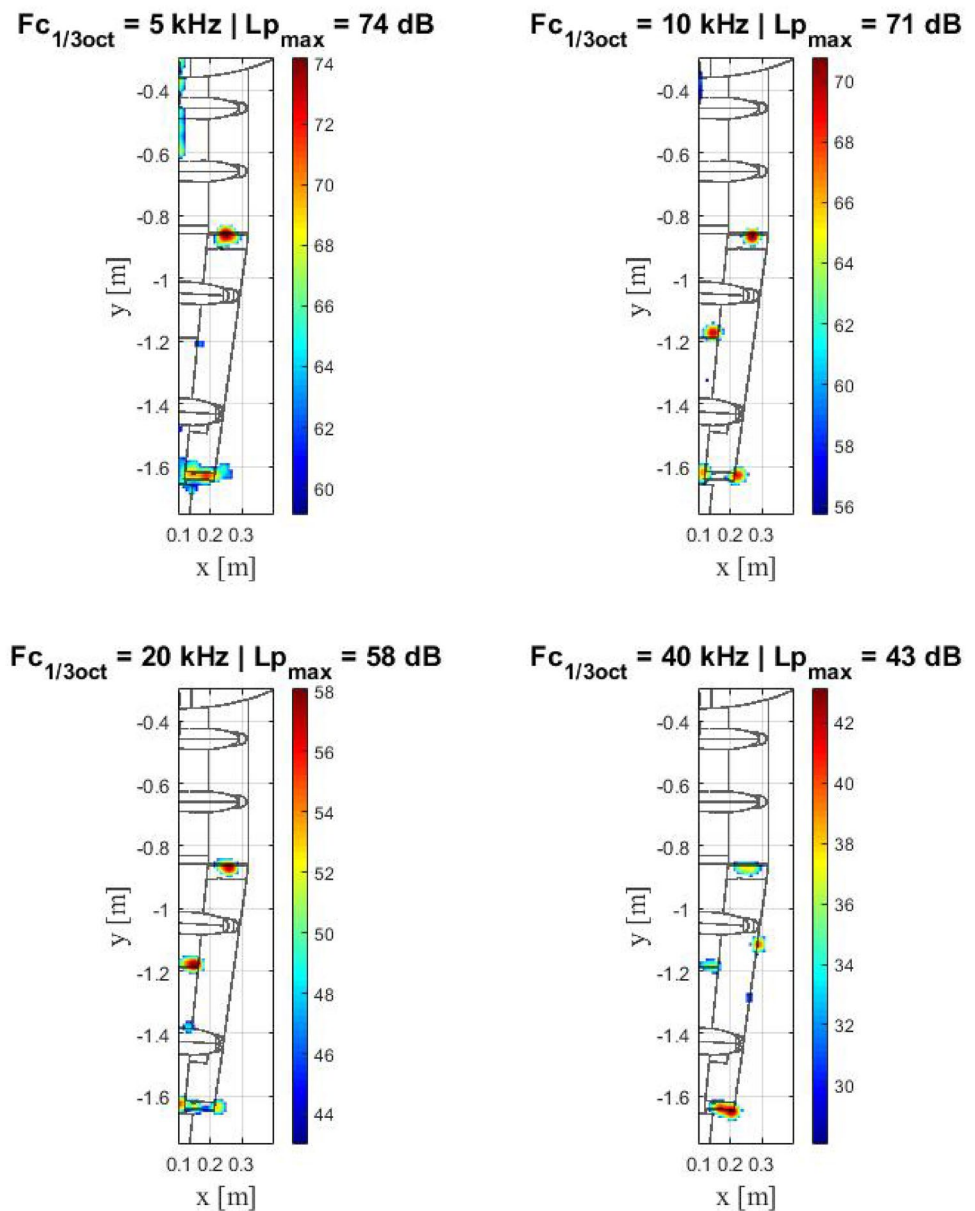


Fig. 17 Lined flap mounted on the left wing in LA configuration



simultaneously acquired through a phased microphone array installed on a flat plate movable on the WT test section floor. Data was post-processed and then analyzed with a conventional beamforming technique and by applying the CLEAN-SC algorithm in order to provide the sources position on scan grid planes covering the areas of interest: propellers, full model, wings, and wing tips.

Like for the aerodynamic study, also the aeroacoustic investigation confirms the expected behavior in terms of noise source location and intensity. The effectiveness of a low-noise device, consisting of a lined flap, has been tested and quantitatively estimated.

The results achieved support the idea that the adopted configuration is promising from both the aerodynamic and

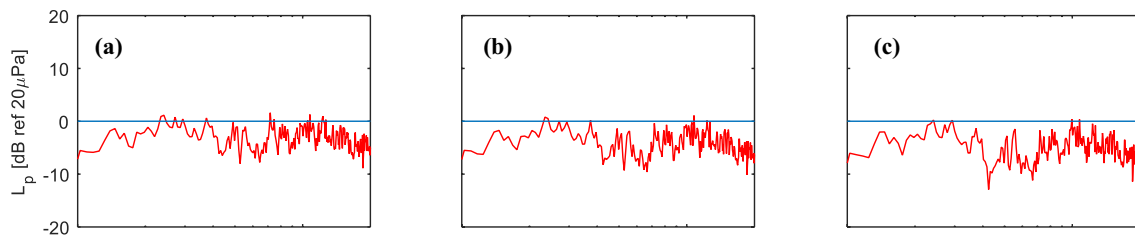


Fig. 18 Noise reduction (L_p) as obtained by the application of the lined flap on the left wing in LA configuration at $U_{nom} = 68$ m/s for $AoA = 0^\circ$ (a), 6° (b) and 8° (c)

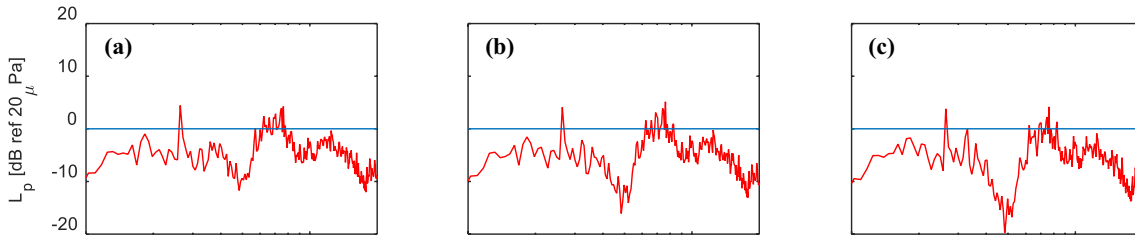


Fig. 19 Same as previous plot (Fig. 17) but for $U_{nom} = 50$ m/s

aeroacoustic viewpoint. The application of a lined flap provided a satisfactory benefit in terms of airframe noise abatement thus supporting the applicability of such a solution in reality. The evaluation of this solution on aircraft flight tests remains a challenge of future studies.

Acknowledgements The experimental test campaigns were founded through EU funded projects LOSITA (JTI-CS-2013-1-GRA-02-020) and WITNESS (JTI-CS-2013-2-GRA-02-025). The authors sincerely acknowledge RUAG and DLR personnel for their essential support during the experiments.

References

- Dugan, J.F., Bencze, D.P., Williams, L.J.: Advanced turboprop technology development. In: Aircraft Systems and Technology Meeting Seattle, WA, U.S.A (1977). <https://doi.org/10.2514/6.1977-1223>
- Dugan, J., Miller, B., Graber, E., Sagerser, D.: The NASA high-speed turboprop program. SAE Trans. **89**, 3397–3415 (1980)
- Borst, H.V.: Summary of propeller design procedures and data. Volume 1. Aerodynamic design and installation. Borst (Henry V) and associates Rosemont pa (1973)
- Johnson, R.P.: An Empirical Method for the Prediction of Airplane Drag Divergence Mach Number. RAND Corporation, Santa Monica, CA (1953). <https://doi.org/10.7249/RM1188>
- Harlamert, W.B., Edinger, R.: Development of an Aircraft Composite Propeller. SAE Trans. **88**(3), 790527–790858 (1979)
- Kong, C., Park, H., Lee K., Choi, W.: A Study on structural design and analysis of composite propeller blade of turboprop for high efficiency and light weight. In: ECCM15—15th European Conference on Composite Materials, Italy (2012)
- Aschwanen, P., Mueller, J., Griiths, R., Smith, B., Northall, R.: Wind tunnel testing of a counter rotating open fan powered aircraft configuration. In: 28th Aerodynamic Measurement Technology, Ground Testing, and Flight Testing Conference, New Orleans, Louisiana (2012). <https://doi.org/10.2514/6.2012-2860>
- Di Marco, A., Burghignoli, L., Centracchio, F., Camussi, R., Ahlefeldt, T., Henning, A., Mueller, J.: Airframe noise measurements in a large hard-walled closed-section wind tunnel. Appl. Acoust. **146**(3), 96–107 (2019)
- Casalino, D., Barbarino, M.: Optimization of a single-slotted lined flap for wing trailing-edge noise reduction. J. Aircr. **49**(4), 1051–1063 (2012)
- Soderman, P.T., Allen, C.S.: Microphone measurements in and out of airstream. In: Mueller, T.J. (ed.) Aeroacoustic measurements. Springer, Heidelberg (2002)
- Oerlemans, S., Broersma, L., Sijtsma, P.: Quantification of airframe noise using microphone arrays in open and closed wind tunnels. Int. J. Aeroacoust. **6**(4), 309–333 (2007). <https://doi.org/10.1260/147547207783359440>
- Sijtsma, P.: Acoustic array corrections for coherence loss due to the wind tunnel shear layer. In: 2nd Berlin Beamforming Conference. Berlin (2008)
- Allen, C., Blake, W.K., Dougherty, R.P., Lynch, D., Soderman, P., Underbrink J.R.: Aeroacoustic measurements. Springer, Heidelberg (2002)
- Ahlefeldt, T.: Aeroacoustic measurements of a scaled half-model at high Reynolds numbers. AIAA J. **51**(12), 2783–2791 (2013)
- Ehrenfried, K., Koop, L.: Comparison of Iterative deconvolution Algorithms for the mapping of acoustic sources. AIAA J. **45**(7), 1584–1595 (2007)
- Yardibi, T., Zawodny, N.S., Bahr, C., Liu, F., Cattafesta, L.N., Li, J.: Comparison of microphone array processing techniques for aeroacoustic measurements. Int. J. Aeroacoust. **9**(6), 733–761 (2010)
- Chu, Z., Yang, Y.: Comparison of deconvolution methods for the visualization of acoustic sources based on cross-spectral

- imaging function beamforming. *Mech. Syst. Signal Process.* **48**(1–2), 404–422 (2014)
18. Sijtsma, P.: CLEAN based on spatial source coherence. *Int. J. Aeroacoust.* **6**(4), 357–374 (2007)
 19. Brooks, T.F., Humphreys, W.M.: A deconvolution approach for the mapping of acoustic sources (DAMAS) determined from phased microphone arrays. *J. Sound Vib.* **294**(4–5), 856–879 (2006)
 20. Ahlefeldt, T., Spher, C., Berkefeld, T., Di Marco, A., Burghignoli, L.: A tomographic directivity approach to frequency domain beamforming. In: 2018 AIAA/CEAS Aeroacoustics Conference Atlanta, Georgia (2018). <https://doi.org/10.2514/6.2018-2808>
- Publisher's Note** Springer Nature remains neutral with regard to jurisdictional claims in published maps and institutional affiliations.